The Astrophysical Journal, 844:24 (5pp), 2017 July 20 https://doi.org/10.3847/1538-4357/aa76e3

Association of Supergranule Mean Scales with Solar Cycle Strengths and Total Solar Irradiance

Sudip Mandal[1], Subhamoy Chatterjee[1], and Dipankar Banerjee[1,2]
[1] Indian Institute of Astrophysics, Koramangala, Bangalore 560034, India; sudip@iiap.res.in
[2] Center of Excellence in Space Sciences India, IISER Kolkata, Mohanpur 741246, West Bengal, India
Received 2017 May 8; revised 2017 May 22; accepted 2017 May 31; published 2017 July 18

Abstract

We analyze the long-term behavior of the supergranule scale parameter, in active regions (ARs) and quiet regions (QRs), using the Kodaikanal digitized data archive. This database provides century-long daily full disk observations of the Sun in Ca II K wavelengths. In this paper, we study the distributions of the supergranular scales, over the whole data duration, which show identical shape in these two regimes. We found that the AR mean scale values are always higher than that of the QR for every solar cycle. The mean scale values are highly correlated with the sunspot number cycle amplitude and also with total solar irradiance (TSI) variations. Such a correlation establishes the cycle-wise mean scale as a potential calibrator for the historical data reconstructions. We also see an upward trend in the mean scales, as has already been reported in TSI. This may provide new input for climate forcing models. These results also give us insight into the different evolutionary scenarios of the supergranules in the presence of strong (AR) and weak (QR) magnetic fields.

Key words: Sun: activity – Sun: chromosphere – Sun: evolution – Sun: granulation – Sun: magnetic fields – solar–terrestrial relations

1. Introduction

Solar cycle refers to the 11 year periodic variation observed in a variety of solar activities such as sunspot number, sunspot area, 10.7 cm radio flux, flare occurrences, number of coronal mass ejections, etc. (See Hathaway 2015 for a complete review on the solar cycle.) Almost all of the phenomena/features on the Sun seem to have this periodicity embedded into their properties. In this paper, we study a chromospheric feature, known as supergranules. These are the large-scale (∼25–30 Mm) velocity (∼400 m s^{-1}) structures on the solar surface, with an average lifetime of 25 hr (Rieutord & Rincon 2010).

The study of supergranules from ground-based telescopes has been of interest since the early 1900s. Though there are reports as early as 1916 (Plaskett 1916), the first confirmation came from Hart (1956), who reported on "velocity fluctuations" having a length scale of 26 Mm. In the following few decades, a lot of work was done on supergranules, including the first confirmation from Doppler images by Leighton et al. (1962). Simon & Leighton (1964) realized that the strong magnetic network-like structures (known as "network boundaries"), seen through a chromospheric Ca II K line, are actually the tracer of supergranule cells. Later, Rast (2003) showed that the evolution of the supergranules triggers the dispersion of the magnetic field stored in these boundaries.

Thus, the first step in analyzing the supergranular properties is to detect these network boundaries from Ca II K images. Several techniques have been applied by many authors to detect the network pattern (hence supergranules): the auto-correlation technique (Sýkora 1970; Hagenaar et al. 1997), fast Fourier transformation (Muenzer et al. 1989), automated skeleton detection (Berrilli et al. 1999), and watershed transformation (McIntosh et al. 2011; Chatterjee et al. 2017). Several properties of the supergranules, such as scale (Srikanth et al. 2000; McIntosh et al. 2011) and fractal dimension (Paniveni et al. 2010), show signatures of a solar-cycle-like variation. In fact, Hagenaar et al. (1997) and Berrilli et al. (1998) showed that the scale distribution follows the voronoi tessellation pattern. Most of these results were derived using a short span of data (less than a solar cycle) or a couple of solar cycles (McIntosh et al. 2011).

The other important connection of the supergranule scale was found by McIntosh et al. (2011), where the authors showed an in-phase variation of the scale parameter, for the 23rd cycle, with the "total solar irradiance" (TSI) cycle. Historically, this TSI was thought to be constant and considered only to be variable in longer time periods (evolutionary timescale of the star). Only after the advent of spaceborne radiometers did it become clear that the TSI varies in much smaller timescales, from days to years (Willson et al. 1981). Since space-based measurements are only available from the 1970s, there are studies that link the historical sunspot observations with the TSI changes on solar cycle timescales (Hudson et al. 1982; Fröhlich & Lean 1998, 2004). Thus, a long-term study of the scale property will enable us to better understand the historical TSI variations.

One of the key constraints in establishing a clear connection between the different supergranular properties with the solar cycles is the non-availability of a long-term uniform, homogeneous data set. The Kodaikanal Solar Observatory (KSO) in India has been accruing Ca II K observations since 1907. For the first time, these images have been used by Chatterjee et al. (2017) to detect the supergranules in an automated manner and derived different properties of them over the span of 100 years (cycles 14–23). These authors found that the supergranule scales and fractal dimension have 11 year solar-cycle-like periodicities persistent throughout the data. One of the highlights of this work is that the opposite correlations of the active and quiet region supergranule scale with the sunspot number cycle.

As a follow-up to Chatterjee et al. (2017), we further explore the properties of the supergranule scale. Section 4.1 presents an investigation of supergranule mean scale variation over two

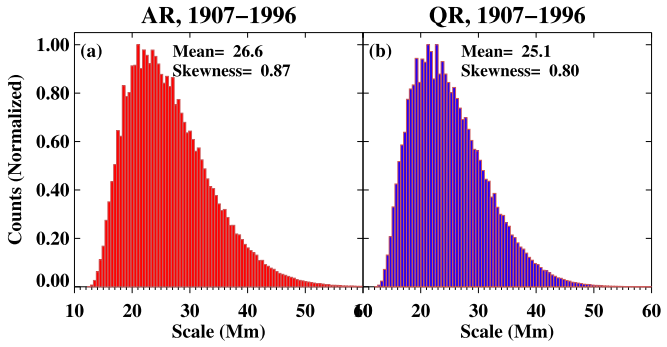

Figure 1. Distributions of the supergranule scales for the AR (a) and the QR (b), respectively. The histograms are constructed from daily observations over the period of 1907–1996.

regions. Long-term association of these scale values with the TSI and the sunspot number has been analyzed in Section 4.2. Next, the variation of the scale parameter within a given cycle is derived in Section 4.3. We conclude by summarizing the main results in Section 5.

2. Kodaikanal Data Description

We used the digitized archive of Ca II K observations captured at KSO, India. Originally, the images were taken in photographic plates, and recently, these plates were digitized in a 4 K × 4 K format at the Indian Institute of Astrophysics. The digitized version of these data is now available for public use at https://kso.iiap.res.in//. These data cover a period of almost 104 years, i.e., from cycle 14 (decline phase only) to cycle 23. As there are a significant number of missing days and plates with poor plate conditions after 1996 (Priyal et al. 2014; Chatterjee et al. 2016), we only consider cycle 14 to cycle 22 in this study.

3. Method

We use the detected network boundary information as obtained by Chatterjee et al. (2017). This feature extraction was done using an automated algorithm based on the "watershed technique" (Lin et al. 2003; McIntosh et al. 2011). We again remind the reader that these network boundaries are the proxies for the supergranular cells (Simon & Leighton 1964). Regions on the Sun have been divided into two regimes: active regions (ARs) and quiet regions (QRs; see Chatterjee et al. 2017 for more details). In this study, we use the scale parameter for each of the supergranules from daily images. The supergranule scale is defined as the radius of the circle whose area is equal to the area of the supergranule (Chatterjee et al. 2017).

4. Results

4.1. Inter-cycle Variations

First, we compare the distribution of the supergranular scale values obtained from daily images over the whole span of the data (cycles 14–22) and separately for ARs and QRs. The normalized histograms are plotted in Figures 1(a) and (b) (red for AR and blue for QR). From the plot we readily notice that the distributions in two regimes are of similar shape (note the closeness of the skewness parameter, 0.87 for AR and 0.80 for QR). This is interesting because the AR and QR represent different magnetic field strengths, and it has been conjectured by Meunier et al. (2008) that the network magnetic elements have a shrinking effect on the supergranules. Also, both of these distributions are similar to the voronoi distribution (Hagenaar et al. 1997). In other words, such a resemblance also indicates the goodness of the automated detection algorithm used by Chatterjee et al. (2017). We also note that the mean of this scale distribution in the AR is higher (26.6 Mm) than that of the QR (25.1 Mm). This is to remind us that these values are calculated over nine solar cycles. This means it is not clearly evident whether such differences in the scales are persistent over all the cycles or just that an anomalous cycle lead to this overall contrast.

We probe such scenarios by calculating the mean scale for every individual cycle for the AR as well as for the QR. While deriving the mean values, we also calculated the uncertainties involved in those values. One of the primary sources of uncertainties is the watershed detection method itself. In fact, McIntosh et al. (2011), who have used this technique first to detect the supergranules, have also performed the error measurements involved in this technique by utilizing 1000 Monte Carlo realizations. Using a Poisson noise model, these authors found that the changes in the mean values are considerably less than the annual and monthly variations in the value itself (they found the variance of the mean value to be ∼0.01 Mm). Thus, we derive the errors of the average values by calculating the "confidence interval" (C.I). As the sample standard deviation is known, so the formula for the (C.I) within which population mean should exist reads as

$$\mathrm{C.I} = \bar{X} + Z^* \times (s/\sqrt{n}), \quad (1)$$

where $\bar{X}$ is the sample mean value, whereas s and n are the standard deviation and the sample size, respectively. Z^* is the multiplier value that is set to 1.96, which corresponds to a C.I of 95%. Now, this number is derived from a normal distribution. From Figure 1, we note that the histograms are not normally distributed (in fact, are positively skewed). Since our sample size is very large (≈60,000), we make use of the same multiplier value according to the "central-limit theorem."

The results are plotted in Figure 2(a). There are quite a few interesting features visible in this plot. First, we notice that the AR mean scale is always higher than that of the QR, for all the cycles. Thus, we confirm the persistence, as questioned in the previous section. Next, we see that both the AR and QR mean scales are oscillating with a common pattern as we go through different cycles. Careful inspection reveals that such variation patterns are also present in sunspot cycles, which we will explore in detail in the following sections.

We again look back at these curves to explore more features from them. Both of the curves seem to ride on an upward moving trend. This feature is particularly interesting as such trends are not common in solar proxies, but are found in TSI from the observations (Willson 1997). Though within our data duration we only have two distinct minima points, we try to quantify the trends by fitting the minimum points with straight lines (dotted lines in Figure 2(a)). In order to estimate these slopes along with the uncertainties, we use the C.I of the mean values as the measurement errors during the linear fitting. For the AR case the slope value is 0.10 ± 0.03 Mm yr^{-1}, whereas for the QR it is 0.07 ± 0.02 Mm yr^{-1}. Thus, the trend is marginally steeper in the AR compared to the QR. Though these slope values are small, but on longer timescales (for example, on decadal timescales), they have a profound effect on the mean scale values.

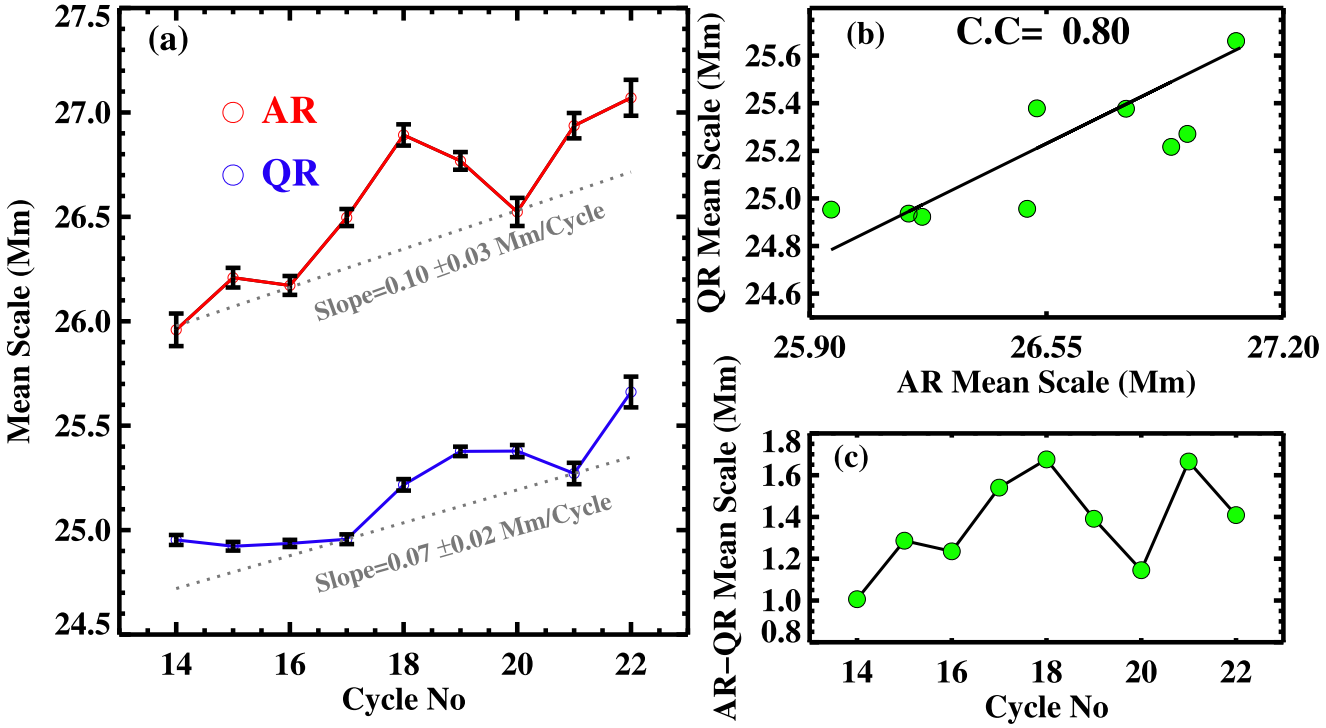

Figure 2. Panel (a) shows the variations of the mean supergranular scales with the solar cycles for AR and QR. The scatter plot between the two is shown in panel (b), whereas differences in the AR and QR mean scales are plotted in panel (c). The error bars in panel (a) represent the 95% confidence limit on the calculated mean scale values.

The two curves show a similar variation with cycles, but there are also some subtle differences. The locations of the maxima and minima of the two curves appear at different cycle numbers. For an example, the maxima for the AR mean scale occurs for the 18th cycle, whereas the QR curve reaches it maximum at the 19th cycle (the same also happens for the minimum). Such small deviations in the two curves result in a correlation value of 0.8 between them as shown in Figure 2(b). We have already seen the dominance of AR mean scales over the QR values, but it is necessary to quantify the difference between the two. In Figure 2(c), we plot the scale difference (AR−QR) with different solar cycles. Interestingly, this difference value reaches its maximum value of 1.7 Mm twice (18th and 21th cycles), whereas the minimum value of 1 Mm) also occurs twice (14th and 20th cycles).

4.2. Relations with Sunspot Number and TSI

We have seen in the previous section that the AR and QR mean scales show oscillatory patterns (with solar cycles) that are similar to the amplitude variation of sunspot cycles. In fact, as mentioned earlier, McIntosh et al. (2011) have shown the association of the scale values with the TSI variation only for the 23rd cycle. In this section, we extend the study using the data over nine solar cycles and build some statistics.

The earliest TSI observations are available only from the 1980s from the Active Cavity Radiometer Irradiance Monitor (ACRIM 1, 2, 3) followed by the Variability of solar IRradiance and Gravity Oscillations (*SOHO*/VIRGO; since 1996) and the Total Irradiance Monitor (SORCE/TIM; since 2003). Within the data period investigated in this paper, we have only one and a half solar cycle data overlap. Thus, we make use of the historical TSI reconstruction model output. The Naval Research Laboratory's Total Solar Irradiance

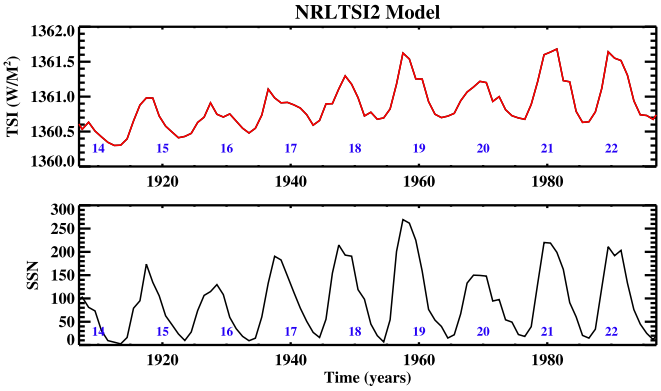

Figure 3. Top panel shows the yearly variation of the TSI obtained from the NRLTSI2 model. The bottom panel shows the same, but for the SSN. Solar cycle numbers are also displayed near the bottom of the panels.

(NRLTSI2.0) historical TSI reconstruction (for the last 400 years) is based on the model by Lean et al. (1995). The NRLTSI data are being produced by NOAA as a Climate Data Record and are available at http://lasp.colorado.edu/home/sorce/data/tsi-data/. The details of the model algorithm and its features are described in Coddington et al. (2016). These model TSI data have also been updated after the revision of the sunspot number (Kopp et al. 2016) and are also scaled to match SORCE/TIM observations. The model output is plotted in Figure 3 along with the yearly SIDC sunspot number data (which are available at http://sidc.oma.be/silso/).

Immediately from Figure 3, we note a clear similarity to Figure 2(a). The TSI also seems to ride on an upward trend with the solar cycles, just like the mean scale curves. In order to have a quantitative measure, we first calculate the peak TSI values (in $W\,m^{-2}$) and peak sunspot number for each of the

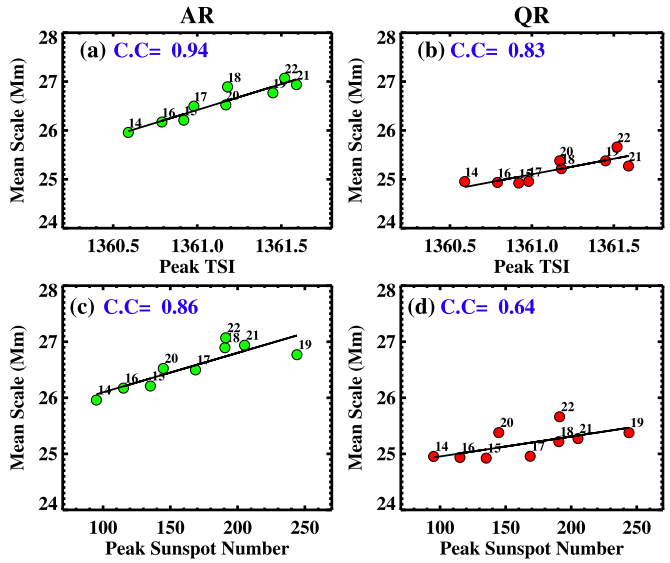

Figure 4. Panels (a) and (b) show the scatter plot between the peak TSI and the mean scale values for different solar cycles, whereas panels (c) and (d) show the scatter plots between the peak SSN and the mean scale values.

cycles from Figure 3. In Figures 4(a) and (b), we show the scatter plots between the peak TSI and the mean scale (for both the regions, AR and QR) calculated for each of the cycles. Now, the correlation coefficients (C.Cs) for the two cases are high but different: for AR it is 0.94, whereas for QR it is 0.83. Such high correlations immediately point toward the possible use of the cycle-wise mean scale as a calibrator for the historical TSI data reconstructions. This has another application, as we have seen that an upward trend is present for both of the curves (TSI and scale). Thus, one can cross-calibrate between the trend values to set better constraints on it, as this trend has an important effect on climate forcing models (Lockwood & Fröhlich 2007).

We also calculated the correlations between the mean scale and the peak sunspot number of the cycles, as shown in Figures 4(c) and (d). Also, in this case, we notice that he AR correlation (C.C = 0.86) is significantly higher than that of the QR. In order to explain the relatively lesser C.C for the QR regime, we note that, from Figure 2, for the initial four cycles (cycles 14–17) the QR scale values did not change (constant at ∼25 Mm), and this may have contributed toward this lower coefficient value. Because there are studies that indicate small differences between sunspot number and sunspot area series (Li et al. 2016), we have thus also computed the correlations between the mean scale and peak sunspot area, and the coefficient values (0.87 for AR and 0.66 for QR) are very similar to the previous values obtained using peak sunspot numbers.

In an interesting observation, we notice that all the C.C values computed with peak SSN are less as compared to the same when obtained with the peak TSI. This means that the overall supergranular scale is better following the TSI cycle amplitude as compared to the sunspot number cycle amplitude. One possible reason behind this could be the linearly increasing trend that is present in both the TSI and the mean scales but not in the SSN.

4.3. Histogram Analysis and Intra-cycle Variations

In the previous two sections, we found that the mean scale values change considerably with different solar cycles, and they have an in-phase amplitude variation with the peak sunspot number and the TSI values. On the other hand, it is expected that the scale distribution will also change within a solar cycle, i.e., on a timescale of ≈11 years. To probe such changes, we construct 2D histograms for the AR and QR and plot them in Figures 5(a) and (b), respectively. The *y*-axes of these plots represent the normalized histograms. The color bar indicates the strength of the histograms. In order to minimize statistical fluctuations, we use yearly data to construct these histograms. Such a 2D histogram not only captures the dominant scale locations over time, but it allows us to study other statistical features such as changes in distribution widths (variance). To highlight these features, we use contours of different levels (or strengths): C1, which outlines the higher (0.85) values, whereas the other two contours, C2 and C3, outline the moderate (0.5) and lower (0.2) values, respectively.

We discuss the AR histogram first (Figure 5(a)). In this case, we see that all three contours show a clear 11 year periodic solar-cycle-like variation. Now, following the C1 contour for a given cycle, we notice a very interesting property. The contour width is large near the start of a cycle. After that it increases by a small amount and then decreases significantly to reach its minimum value near the end of the cycle. This means that such a variation is not symmetric with the cycle duration, which is not a common case for the solar proxies (e.g., sunspot number or with sunspot area cycle). In another observation, we note that the variations near the wings of the distributions (in C2 and C3) are more prominent compared to the core of the distributions. In this case, these variations follow the shape of the solar cycles that eventually leads to an in-phase alteration of the variance.

Time evolution of the QR histogram (Figure 5(b)) is different from the AR case, however. We note that the width of the C1 contour changes very little with the evolution of a cycle. Such a (near) constant width indicates that the the core of the distribution does not change with solar cycle. Though we must again highlight that the effect of the missing data, for the past couple of years, is evident in the last cycle (cycle 22). On the other hand, the widths of the other two curves (C2 and C3) do show a small amplitude anti-correlation trend with the solar cycles (as the variation in this case is ∼1 Mm, thus the anti-correlation behavior appears small in the axis range used in the plot). Thus, the anti-correlated behavior of the QR scale with the solar cycle, as found by Chatterjee et al. (2017), is mainly contributed by the wings of the QR scale distributions.

5. Summary and Conclusion

In this paper, using the Kodaikanal digitized Ca II K data, we investigated the long-term (cycle-wise) behavior of the supergranule scales over multiple solar cycles. Below, we summarize the main results from our analysis.

1. We find that the supergranule mean scales, in the AR and QR, over a long period of time (nine solar cycles), show similar kinds of distributions. We also find that the mean scale of the AR is higher than that of the QR, and the difference between the two has a maximum value of ≈1.8 Mm.
2. Calculations of the mean scale, for each of the solar cycles, reveal an oscillating pattern for both the AR and QR. Both of these curves depict an upward moving trend that is steeper in the AR as compared to the QR. Also, we

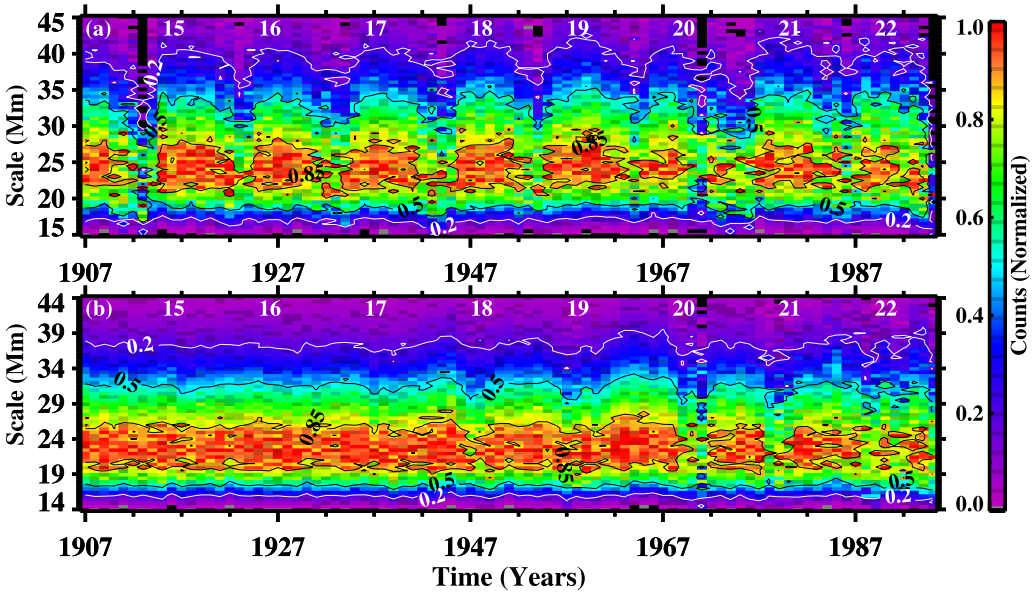

Figure 5. 2D histograms for the AR (a) and QR (b), respectively. Different contours indicate the normalized histogram values. See the text for details.

find that the AR mean scale is persistently higher than QR during all the cycles (∼90 years) investigated in this study. Though there exists a relatively high correlation between the two, we also find that there are some differences in terms of the location of the maxima and minima of the mean scale curves.

3. We find that these mean scales are significantly correlated with the peak TSI values. This makes them a potential calibrator for historical TSI reconstructions. The peak sunspot numbers are also correlated well with the mean scales. Interestingly, the C.Cs in both the cases are higher in the AR as compared to the QR. Among them, we also obtain higher correlations between mean scale and peak TSI as compared to mean scale and peak sunspot number.
4. The intra-cycle variation of the scale values are also investigated using 2D histograms. We note an in-phase variation for the AR scale with the solar cycle cycle, whereas the same for the QR are anti-correlated. The spread in the AR scale distribution is found to be higher near the start of a cycle and becomes narrower at the end of it, whereas for the QR, the width remains almost invariant.

In conclusion, we find that the properties of the AR and QR (mean) scales are quite different and have different relations with solar cycles. The correlation values indicate the possibility of using the cycle-wise mean scale as a historical TSI calibrator. Future studies using data from other observatories will greatly help in constraining these relations, which can further be used by modelers for better accuracy in model output.

The authors would like to thank the referee for valuable suggestions that helped to improve the quality and the presentation of the paper. We would like to thank the Kodaikanal facility of the Indian Institute of Astrophysics, Bangalore, India for proving the data. The data series is now available for public use at http://kso.iiap.res.in/data. We also thank the Science & Engineering Research Board (SERB) for the project grant (EMR/2014/000626).

References

Berrilli, F., Ermolli, I., Florio, A., & Pietropaolo, E. 1999, A&A, 344, 965
Berrilli, F., Florio, A., & Ermolli, I. 1998, SoPh, 180, 29
Chatterjee, S., Banerjee, D., & Ravindra, B. 2016, ApJ, 827, 87
Chatterjee, S., Mandal, S., & Banerjee, D. 2017, arXiv:1705.00175
Coddington, O., Lean, J. L., Pilewskie, P., Snow, M., & Lindholm, D. 2016, BAMS, 97, 1265
Fröhlich, C., & Lean, J. 1998, GeoRL, 25, 4377
Fröhlich, C., & Lean, J. 2004, A&ARv, 12, 273
Hagenaar, H. J., Schrijver, C. J., & Title, A. M. 1997, ApJ, 481, 988
Hart, A. B. 1956, MNRAS, 116, 38
Hathaway, D. H. 2015, LRSP, 12, 4
Hudson, H. S., Silva, S., Woodard, M., & Willson, R. C. 1982, SoPh, 76, 211
Kopp, G., Krivova, N., Wu, C. J., & Lean, J. 2016, SoPh, 291, 2951
Lean, J., Beer, J., & Bradley, R. 1995, GeoRL, 22, 3195
Leighton, R. B., Noyes, R. W., & Simon, G. W. 1962, ApJ, 135, 474
Li, K. J., Li, F. Y., Zhang, J., & Feng, W. 2016, SoPh, 291, 2917
Lin, G., Adiga, U., Olson, K., et al. 2003, Cytometry Part A, 56A, 23
Lockwood, M., & Fröhlich, C. 2007, RSPSA, 463, 2447
McIntosh, S. W., Leamon, R. J., Hock, R. A., Rast, M. P., & Ulrich, R. K. 2011, ApJL, 730, L3
Meunier, N., Roudier, T., & Rieutord, M. 2008, A&A, 488, 1109
Muenzer, H., Schroeter, E. H., Woehl, H., & Hanslmeier, A. 1989, A&A, 213, 431
Paniveni, U., Krishan, V., Singh, J., & Srikanth, R. 2010, MNRAS, 402, 424
Plaskett, H. H. 1916, ApJ, 43, 145
Priyal, M., Singh, J., Ravindra, B., Priya, T. G., & Amareswari, K. 2014, SoPh, 289, 137
Rast, M. P. 2003, ApJ, 597, 1200
Rieutord, M., & Rincon, F. 2010, LRSP, 7, 2
Simon, G. W., & Leighton, R. B. 1964, ApJ, 140, 1120
Srikanth, R., Singh, J., & Raju, K. P. 2000, ApJ, 534, 1008
Sýkora, J. 1970, SoPh, 13, 292
Willson, R. C. 1997, Sci, 277, 1963
Willson, R. C., Gulkis, S., Janssen, M., Hudson, H. S., & Chapman, G. A. 1981, Sci, 211, 700